RSC Advances

ARTICLE

3D Interconnected Hierarchically Macro-mesoporous TiO_2 Network Optimized by Biomolecular Self-assembly for High Performance Lithium Ion Battery

Received 00th January 20xx,
Accepted 00th January 20xx

DOI: 10.1039/x0xx00000x

www.rsc.org/

Xiao-Ning Ren,[†a] Liang Wu,[†a] Jun Jin,[a] Jing Liu,[a] Zhi-Yi Hu,[b] Yu Li,[*a] Tawfique Hasan,[c] Xiao-Yu Yang,[a] Gustaaf Van Tendeloo[b] and Bao-Lian Su[*a,d,e]

Biomolecular self-assembly is an effective synthesis strategy for materials fabrication with unique structural complexity and properties. For the first time, we intergrate inner-particle mesoporosity in a three-dimensional (3D) interconnected macroporous TiO_2 structure via the mediation of biomolecular self-assembly of the lipids and proteins from rape pollen coats and P123 to optimize the structure for high performance lithium storage. Benefitting from the hierarchically 3D interconnected macro-mesoporous structure with high surface area, small nanocrystallites and good electrolyte permeation, such unique porous structure demonstrates superior electrochemical performance, with high initial coulombic efficiency (94.4% at 1C) and a reversible discharge capacity of 161, 145, 127 and 97 mA h g^{-1} at 2, 5, 10 and 20C for 1000 cycles, with 79.3%, 89.9%, 90.1% and 87.4% capacity retention, respectively. Using SEM, TEM and HRTEM observations on the TiO_2 materials before and after cycling, we verify that the inner-particle mesoporosity and the $Li_2Ti_2O_4$ nanocrystallites formed during the cycling process in interconnected macroporous structure largely enhance the cycle life and rate performance. Our demonstration here offers opportunities towards developing and optimizing hierarchically porous structures for energy storage applications via biomolecular self-assembly.

1 Introduction

Rechargeable lithium-ion batteries (LIBs) with high storage capacity and cycling stability are considered to be the versatile, clean and promising energy source for next generation portable electronic devices, hybrid electric vehicles (HEV) and electric vehicles (EV).[1] TiO_2 is an attractive alternative to graphite due to its low volume change (3-4%)[2] and relatively high lithium insertion/extraction voltage (~1.7 V). This allows better overcharge protection and safety by avoiding the formation of solid-electrolyte interphase (SEI) layers and lithium electroplating during cycling.[2] Moreover, TiO_2 is suitable for energy storage owing to its abundance, low cost and low impact on environment.[3]

Theoretically, lithium intercalating into anatase TiO_2 can approach to $Li_{0.96}TiO_2$ composition, with a maximum capacity of ~335 mAh g^{-1}. However, phase transition from the original tetragonal phase to orthorhombic symmetry caused by the elastic interaction force between the intercalated lithium ions (Li^+) and formation of weak Ti-Ti interactions leads to only ~0.5 Li^+ insertion per unit of TiO_2 with a practical reversible capacity of 167 mAg^{-1}.[4] It has been demonstrated that the porosity in TiO_2 can improve its cycling stability and capacity at high charge-discharge rates.[5, 6] Indeed, porous TiO_2 structures, with their high surface area, narrow pore-size distribution and good electrolyte permeation have attracted significant interests for LIBs.[7-11] Assembling nanosized TiO_2 such as nanofibers[12], nanorods and nanoparticles[12-14] to hierarchically porous micro/nanostructures is therefore a very effective approach toward the development of high performance TiO_2 electrodes.[15]

In the context of hierarchically porous structure design, mother nature has already provided us with optimized one-, two-, and three-dimensional (1D, 2D and 3D) elaborate architectures, ranging from nanoscale to macroscale,[16] inspiring us to design novel hierarchically porous materials via biotemplating.[17, 18] In general, pollen coats cover the surface of pollen grains and are typically macroporous structures.[19] The lipids and proteins in pollen coats not only allow self-assembly of biomolecules for the formation of hierarchical biostructures, but also bind metal ion precursors for the fabrication of organic or inorganic nanostructures.[20-22] It is widely known

[a] *Laboratory of Living Materials at the State Key Laboratory of Advanced Technology for Materials Synthesis and Processing, Wuhan University of Technology, 122 Luoshi Road, 430070, Wuhan, Hubei, China; Email: yu.li@whut.edu.cn; baoliansu@whut.edu.cn.*
[b] *EMAT (Electron Microscopy for Materials Science), University of Antwerp, 171 Groenenborgerlaan, B-2020 Antwerp, Belgium.*
[c] *Cambridge Graphene Centre, University of Cambridge, 9 JJ Thomson Avenue, Cambridge CB3 0FA, United Kingdom*
[d] *Laboratory of Inorganic Materials Chemistry (CMI), University of Namur, 61 rue de Bruxelles, B-5000 Namur, Belgium; E-mail: bao-lian.su@unamur.be*
[e] *Department of Chemistry and Clare Hall, University of Cambridge, Cambridge CB21 EW, United Kingdom; E-mail: bls26@cam.ac.uk*
† These two authors contributed equally to this work.
Electronic Supplementary Information (ESI) available: Charge and discharge curves of RPC TiO_2 and RPC-P TiO_2 for 100 cycles at 1C, SEM and TEM images of RPC TiO_2, HRTEM image of RPC TiO_2 after 1000 cycles at 2C. See DOI: 10.1039/x0xx00000x

that lipids and proteins can self-assemble to porous membranes under appropriate conditions.[19] It is therefore possible that the lipids and proteins in pollen coats can self-assemble to porous structures. In our previous study, we showed that the inner-particle mesoporosity in 3D ordered macro-mesoporous (3DOMM) TiO_2 can improve cycle life and rate capability for LIBs by 14.3% at 1C for 200 cycles and 10.1% at a rate density of 1C, respectively.[23] Therefore, it is conceivable that the optimizing hierarchically structured porous TiO_2 via self-assembly of the lipids and proteins from pollen coats should offer a new materials synthesis strategy for advanced LIBs.

Herein, we report synthesis of 3D interconnected macroporous TiO_2 (RPC-P TiO_2) with inner-mesopores via biomolecule-mediated self-assembly of the lipids and proteins from rape pollen coats (RPC) (Scheme 1a). Such optimized unique, hierarchical structure with inner-particle mesopores in macroporous structure of RPC-P TiO_2 demonstrates superior electrochemical performance, with high initial coulombic efficiency (94.4% at 1C) and a discharge capacity of 161, 145, 127 and 97 mAh g^{-1} at 2, 5, 10 and 20C after 1000 cycles, with a 79.3%, 89.9%, 90.1% and 87.4% capacity retention, respectively, for the same battery. The as-prepared RPC-P TiO_2 material demonstrates much better performance than our previous work [23] and other reported works for LIBs.[12-14,24]

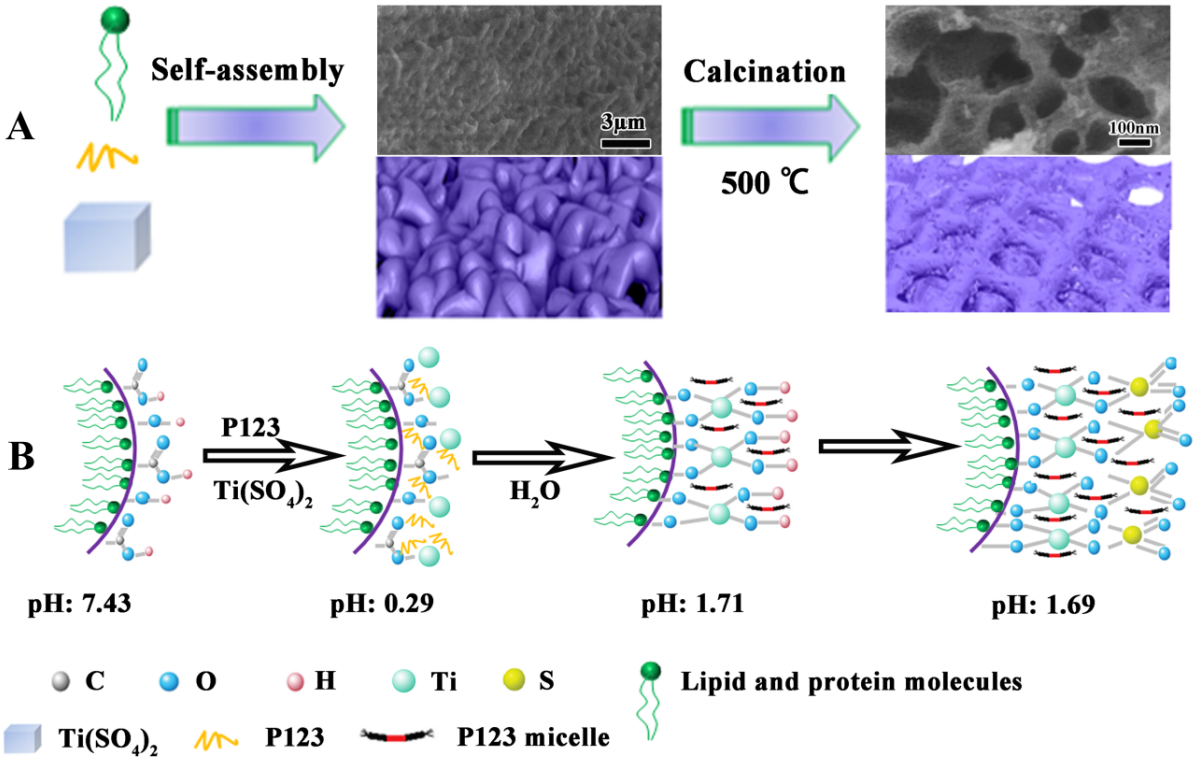

Scheme 1. A: Schematic illustration of the preparation process of RPC-P TiO_2; B: Schematic illustration of the self-assembly process. The grey images in A are the corresponding SEM images.

2 Experimental Section

Synthesis of RPC-P TiO_2

Rape pollen (5g) is dispersed in anhydrous ethanol (50ml) and continuously stirred for 24h. After infiltration, the slight yellow solution containing pollen coats is obtained. The titania precursor solution is produced by dissolving $Ti(SO_4)_2$ (8g) into anhydrous ethanol (100ml). First, 0.4g P123 is dissolved into 40ml pollen coat solution. Next, the titania precursor solution (10ml) is poured into the 40ml pollen coat solution, followed by continuous stirring for 2h. Distilled water (40ml) is then added into the solution, immediately forming reddish brown floccules. The homogeneous mixture is then transferred into Petri dishes. The dishes are kept at room temperature for 12h and then dried at 40°C in air for 24h. Finally, the black brown floccules are transferred to oven at 500 °C for 6h. After the oven is cooled down naturally at room temperature, white powders are collected for further characterization and experimentation.

Synthesis of RPC TiO_2

The above process followed for RPC-P TiO_2 is also used to synthesize RPC TiO_2. The only difference is that P123 is not added in the pollen coat solution.

Characterizations

The crystalline structure of the samples is collected using powder XRD (Bruker D8 Advanced diffractometer, Cu Kα

radiation, λ=1.54056 Å). Field emission scanning electron microscopy (FESEM, Hitachi S-4800), transmission electron microscopy (TEM) and high-resolution transmission electron microscopy (HRTEM) are carried out on a FEI Titan 80-300 "cubed" microscope with double-correctors operated at 300 kV (For RPC-P TiO_2) and JEM-2100F operated at 200 kV (For RPC-TiO_2). Nitrogen adsorption-desorption isotherms are obtained using a Tristar II 3020 surface area and porosity analyzer (Micromeritics, USA). The specific surface area and pore-size distribution are calculated by the Brunauer-Emmett-Teller (BET) method and Barret-Joyner-Halenda (BJH) method, respectively.

Electrochemical Characterization

The working electrode is fabricated by mixing the active material (as-prepared TiO_2), acetylene black, and polyvinylidene fluoride (PVDF) binder in a 7: 2: 1 weight ratio. The resulting slurry is pressed and dried at 120 °C for 12h under vacuum. CR2025 coin-type cells are assembled in a glove box under argon atmosphere. The geometrical area of the electrode is 2.0 cm^2 and the weight of the active material is ~5 mg. Lithium foil is used as both counter electrode and the reference electrode. A 1M solution of $LiPF_6$ in ethylene carbonate and dimethyl carbonate (1:1 in volume) is used as the electrolyte with a Celgard membrane as the separator. The charge-discharge experiments are performed using a LAND battery tester (CT2001A) within a voltage range of 1-3V (vs. Li/Li^+) at various current densities. Electrochemical impedance spectra (EIS) are measured with an electrochemical workstation (Autolab PGSTAT 302N) from 100 kHz to 10 mHz.

3 Results and discussion

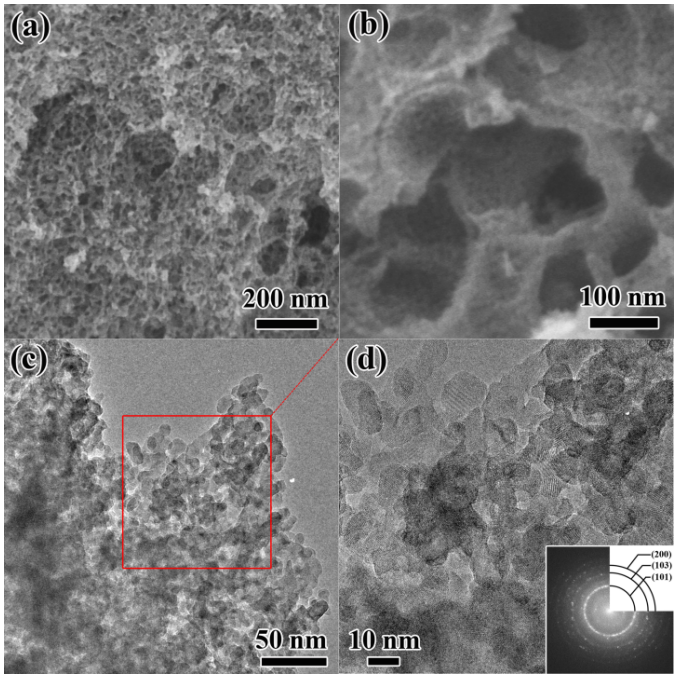

Figure 1. (a, b) SEM, (c) TEM and (d) HRTEM images and SAED pattern (inset) of the as-synthesized RPC-P TiO_2.

It is known that the organic groups, mainly hydroxyls in the pollen coat can interact with metal ions and lead a selective growth in the framework.[25] In our case, the Ti^{4+} first adsorbs on the surface of the pollen coat and gradually converts to titanium hydroxides with water added in the reaction system. During the reaction process, P123 can form micelles to insert into the formed titanium hydroxides on the pollen coat, leading to inner-particle mesopores appearance (Scheme 1b). Finally, 3D optimized hierarchically macro-mesoporous TiO_2 structure can be formed *via* self-assembly of the lipids and proteins from rape pollen coats.

Figure 1a presents the SEM image of RPC-P TiO_2, showing the 3D interconnected macroporous structure. The average dimension of the interconnected macropore is ~100 nm. Figure 1b displays the small nanoparticles constructed macroporous structure. Low magnification TEM image shows that the nanoparticles tightly aggregate to form the inner-particle mesopores in the 3D interconnected macroporous structure (Figure 1c), which is quite different from the inter-particle constructed mesoporous structure (also called worm-like mesopores).[23] The nanoparticles have an average size of ~8nm. The HRTEM image (Figure 1d) clearly demonstrates the mesopores inside the nanoparticles, revealing the existence of inner-particle mesoporosity. The inserted selected area eletron diffraction (SAED) pattern in Figure 1d shows the (200), (103) and (101) crystal planes of anatase TiO_2, consistent with the XRD results (Figure 2).

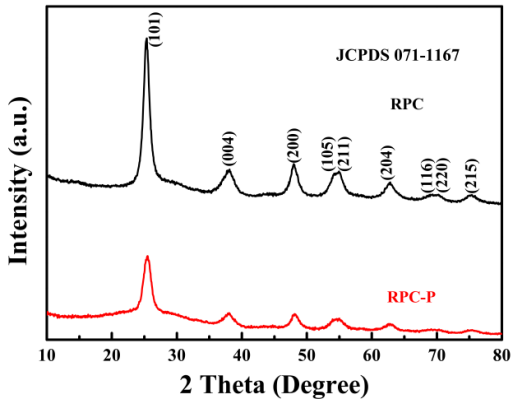

Figure 2. XRD patterns of the as-prepared RPC TiO_2 and RPC-P TiO_2.

The N_2 isotherm of RPC-P TiO_2 with a type H3 hysteresis loop indicates the mesoporous structure (Figure 3a).[26] The BET specific surface area is 129.8 $m^2\ g^{-1}$, which is higher than the TiO_2 prepared with electrospinning technique method of 34-39 $m^2\ g^{-1}$,[12] and melton salts method of 80 m^2g^{-1}.[13] The pore size distribution is ~4 nm (Figure 3b). Such unique inner-particle mesopores inside the macroporous structure can facilitate the electrolyte permeation, leading to a fast transportation of Li^+ ions.[27, 28] Indeed, with the small crystallite-constructed 3D interconnected macropores and inner-particle mesopores, RPC-P TiO_2 offers a bicontinuous transport path and a short path length for Li^+ diffusion. The mesoporosity in RPC-P TiO_2 is also capable of supporting the structure under volume variation during the Li^+ insertion and extraction, resulting in a

relatively high reversible capacity and excellent cycling performance.[28-31]

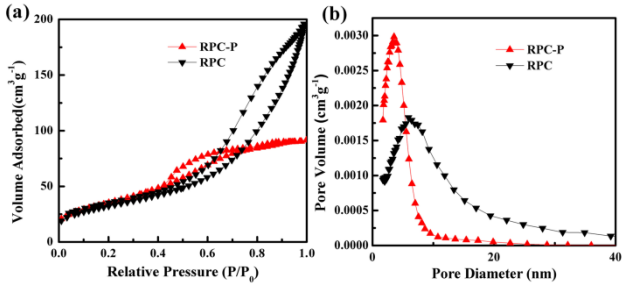

Figure 3. (a) N_2 adsorption-desorption isotherms and (b) BJH pore size distribution plots of the as-prepared RPC TiO_2 and RPC-P TiO_2 respectively.

The electrochemical performance of RPC-P TiO_2 is evaluated in CR2025 coin-type cells. Figure 4a presents the charge and discharge profiles at a current density of 0.2C (1C = 167 mA g^{-1}) for the first four cycles. The plots exhibit two obvious voltage plateaus at ~1.75 and ~1.95V during the discharge and charge processes for cathodic and anodic scan, respectively corresponding to $Ti^{4+/3+}$ redox couple. The Li^+ insertion process can be divided into four stages.[32] The first stage corresponds to a small amount topotactic insertion into the surface structure of the anatase, depending on its crystallite size and surface area. The second stage at ~1.75V represents Li^+ insertion into the interstitial sites of TiO_2 crystal structure. The number of Li^+ ions inserted into the crystalline lattice of anatase is determined by the length of biphasic region.[23] The last two stages can be divided into two regions (1.75-1.5V and 1.5V-1.0V) , showing gradual decay of the voltage after the plateau region represents further topotactic insertion forced by the applied potential.[23] The reverse process takes place during Li^+ extraction. During the initial charge process, a minor difference is observed between 1.6-1.95V for the as-prepared RPC-P TiO_2 due to different Li de-insertion reaction from the amorphous nature of TiO_2.[13] The initial 293 mAh g^{-1} discharge capacity and the subsequent 242 mAh g^{-1} charge capacity shows 17.5% reversible capacity loss, much lower than the best values reported in literature of ~24.2% capacity loss.[33, 34] The discharge and charge capacities for the second cycle are 241 and 234 mAh g^{-1}, respectively, leading to a high coulombic efficiency of 97%. The coulombic efficiency is further increased to 98% for the third cycle and to 99.6% for the fourth cycle. Such high coulombic efficiency for the initial cycles indicates fast Li^+ insertion and extraction balance in the discharge-charge processes in macro-mesoporous RPC-P TiO_2.

Figure 4b presents the cycling performance of RPC-P TiO_2 at 1C for 200 cycles. We obtain an initial discharge and charge capacity of 209 and 197mAh g^{-1}, respectively, resulting in an initial coulombic efficiency of 94.4%. After the second cycle, the coulombic efficiency is increased to ~100%. Figure S1 shows the discharge and charge profiles of RPC-P TiO_2 at 1C for the 1st, 50th, 100th and 200th cycles, demonstrating very stable capacities. A reversible discharge capacity of 186 mAh g^{-1} is maintained after 200 charge-discharge cycles, representing a high 88.8% capacity retention. The coulombic efficiency is ~100% during the charge-discharge process. These results indicate that the 3D interconnected macro-mesoporous TiO_2 structure via biomolecular self-assembly optimizing is very suitable for high rate performance LIBs.

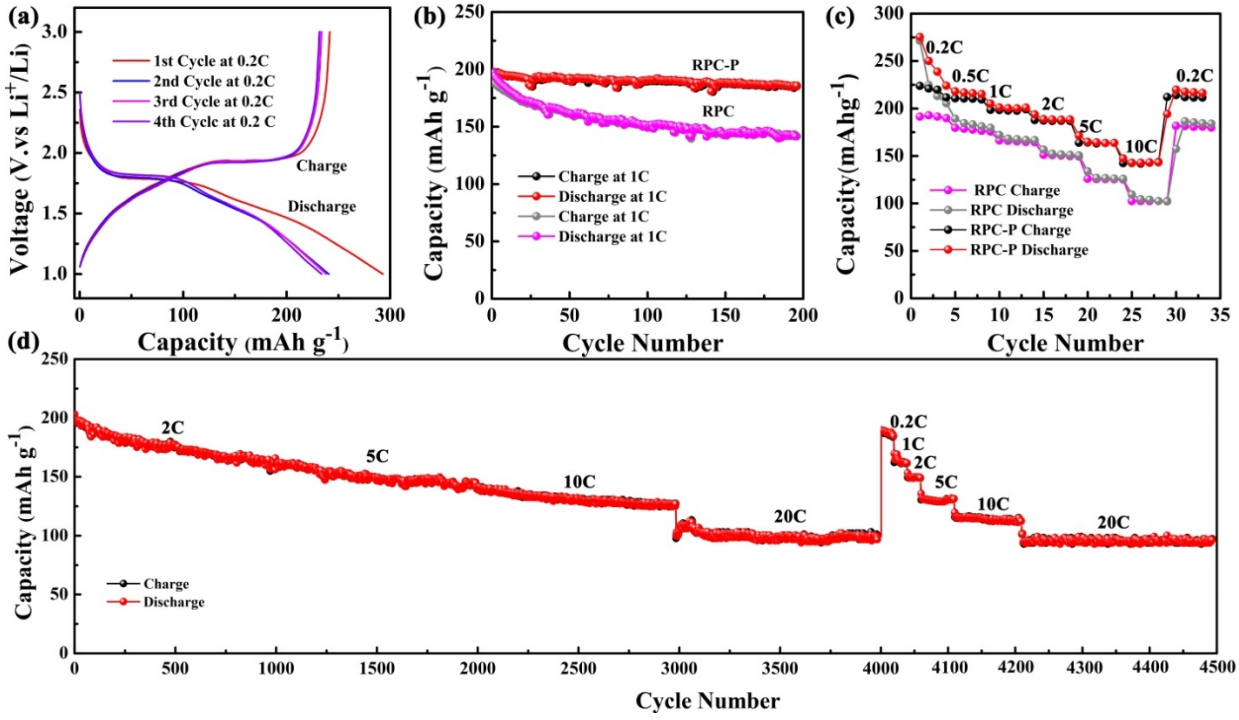

Figure 4. (a) Charge-discharge profiles of RPC-P TiO_2 at 0.2C for the first four cycles, (b) cycling performance of RPC TiO_2 and RPC-P TiO_2 at 1C for 200 cycles, (c) rate performance of RPC TiO_2 and RPC-P TiO_2 electrodes and (d) cycling performance of RPC-P TiO_2 at 2, 5, 10 and 20C for 1000 cycles respectively, and rate performance after cycled at 2, 5, 10 and 20C for 4000 cycles.

Figure 4c plots the rate performance of RPC-P TiO_2 electrode at various charge-discharge rates. The corresponding reversible discharge capacities at 0.2, 0.5, 1, 2, 5 and 10C are 275, 218, 201, 189, 165 and 143 mAh g^{-1}, respectively. A reversible capacity of 220 mAh g^{-1} is achieved when discharge capacity is moved back to 0.2C. We attribute the high capacities at various rates to the small crystallites and high specific surface area with inner-particle mesoporosity in macroporous RPC-P TiO_2, leading to a shorter path length, large number of bicontinuous transport path and good contact with the electrolyte for Li^+ diffusion and insertion.

To verify the advantage of the inner-particle mesoporosity in the 3D interconnected macroporous structure, we also synthesized the 3D interconnected macroporous TiO_2 structure (RPC TiO_2) with inter-particle mesopores. The XRD pattern indicates the anatase phase of RPC TiO_2 (Figure 2). SEM and TEM images show larger macropore and crystallite size with inter-particle mesoporosity (Figure S2). Its BET specific surface area is 115.4 m^2 g^{-1} with an inter-particle mesopore of ~7nm (Figure 3). Its surface area is also higher than the previous TiO_2,[12,13] indicating that the biotemplating method is very suitable for high surface area porous nanostructure preparation. Figure 4b also compares the cycling performance of RPC TiO_2 against RPC-P TiO_2 at 1C, showing a discharge capacity of 142 mAh g^{-1} with only 74.5% capacity retention for 200 cycles. The charge and discharge curves at the 1st, 50th, 100th and 200th cycle of RPC TiO_2 are also presented in Figure S1. Both the discharge capacity and charge capacity of RPC-P TiO_2 are much higher than those of RPC TiO_2. Figure 4c shows the rate performance of RPC TiO_2, demonstrating its lower performance compared to RPC-P TiO_2. Indeed, all the results show that the electrochemical performance of 3D interconnected macroporous RPC-P TiO_2 with inner-particle mesoporosity is superior to 3D interconnected macroporous RPC TiO_2 with inter-particle mesoporosity.

To show the high electrochemical performance of RPC-P TiO_2 for LIBs, the continuous cycle performance of RPC-P TiO_2 at 2, 5, 10 and 20C for 1000 cycles is studied, respectively. At the current desity of 2C, the initial discharge capacity is 203 mAh g^{-1}. The discharge capacity is 161 mAh g^{-1} at the 1000th cycle, demonstrating 79.3% capacity retention. The coulombic efficiency is ~100% after the second cycle (Figure 4d). At the current density of 5C, the initial discharge capacity is 161 mAh g^{-1} and reversible discharge capacity is 145 mAh g^{-1} after 1000 cycles, showing 89.9% capacity retention and ~100% coulombic efficiency. At the current density of 10C, the reversible discharge capacity is 127 mAh g^{-1} at the 1000th cycle with 90.1% capacity retention. The coulombic efficiency is ~100%. At the current density of 20C, a reversible discharge capacity of 97 mAh g^{-1} is obtained after 1000 cycles, displaying 87.4% capacity retention. The coulombic efficiency is still ~100%. After continuous 4000 cycles at different rates, the battery is reset to 0.2, 1, 2, 5, 10 and 20C to study the reversible ability of the RPC-P TiO_2 electrode. When shift to 0.2, 1, 2, 5, 10 and 20C, the discharge capacity is 190, 165, 150, 132, 116 and 95 mAh g^{-1}, demonstrating fabulous reversible performance. This result is much better than our previous work [23] and other reported works.[12-14,24] Thus, the RPC-P TiO_2, with 3D interconnected macro-mesoporous structure presents not only high intial coulombic efficiency but also remarkable specific capacity, outstanding cycling stability and excellent rate performance for several thousand cycles.

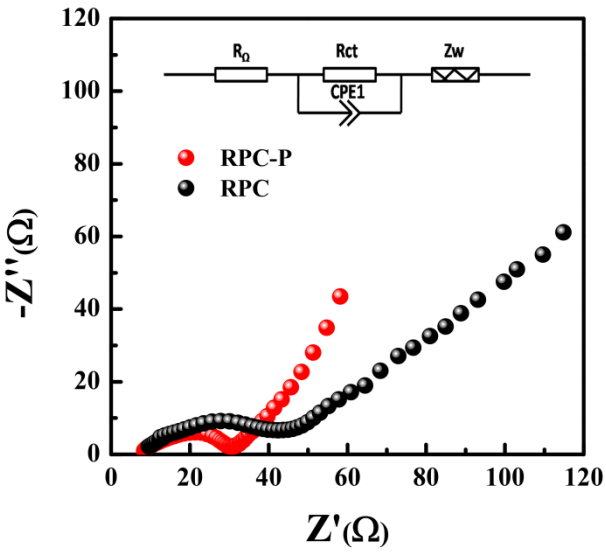

Figure 5. The Nyquist plots of RPC-P TiO_2 and RPC TiO_2 at 0.2C after 10 cycles, indicating the low R_{ct} of the RPC-P TiO_2 electrode.

To further reveal the electrochemical performance and provide dynamic process information of the RPC-P TiO_2 and RPC TiO_2 electrodes, electrochemical impedance spectroscopy (EIS) measurment is carried out. The EIS measurments of RPC-P TiO_2 and RPC TiO_2 are carried out after 10 galvanostatic discharge-charge cycles at 0.2C. The Nyquist plots of the RPC-P TiO_2 and RPC TiO_2 electrodes display one semicircle in the high and middle frequency regions (Figure 5). The semicircles of RPC-P TiO_2 and RPC TiO_2 at the high and middle frequency regions include the surface film resistance (R_{sf}) corresponding to the formation of SEI layer and the charge transfer resistance (R_{ct}) corresponding to the Li^+ charge-transfer resistance at the interface between the elctrode and electrolyte.[35-37] As there is no SEI layer formed in TiO_2, the surface resistance (R_{sf}) is thus negligible. Namely, the semicircles of RPC-P TiO_2 and RPC TiO_2 can be assigned to charge transfer resistance (R_{ct}). The straight slope in the low frequency region corresponds to the solid-state diffusion of the lithium (Z_w).[23] Obviously, the RPC-P TiO_2 electrode has lower resistance than the RPC TiO_2 electrode. Therefore, the RPC-P TiO_2 electrode exhibits a more rapid charge transfer and better performance than the RPC TiO_2 electrode.[38] We attribute this to the higher specific surface area, smaller nanocrystallites and the unique inner-particle mesopores in 3D macroporous RPC-P TiO_2.

To understand the Li^+ storage property and the stability of this structure, SEM and TEM observations of the RPC-P TiO_2 electrode after 1000 cycles at 2C are performed (Figure 6). The SEM images show that the 3D interconnected macroporous structure could still be maintained (Figure 6a), indicating a very

stable macroporous structure. Figure S3 shows that the inner-particle mesopores are also retained in the walls of the macropores, indicating a very stable inner-particle mesoporous structure as well. In TEM observations, we find that after lithiation, some small nanoparticles appear in the porous structure (Figure 6b). According to the previous report[39,40] and our recent findings,[42-44] the nanoparticles are $Li_2Ti_2O_4$ nanocrystallites, which contribute to improvement both in capacity and rate cycling performance. Figure 6c presents the HRTEM image of the squared $Li_2Ti_2O_4$ nanoparticle shown in Figure 6b. The well-defined lattice fringes displays a spacing of 2.09Å, corresponding to the (400) crystal plane of cubic $Li_2Ti_2O_4$ (space group: *F3m3*, lattice constants: a = b = c = 8.375 Å), confirming the composition of these nanocrystallites.

On the basis of the above results, we propose that the Li^+ can quickly intercalate into the porous TiO_2, leading to Li_xTiO_2 formation. With further Li^+ insertion into the Li_xTiO_2 matrix, new $Li_2Ti_2O_4$ nanocrystallites form in the macroporous walls as schemed in Figure 6d. These $Li_2Ti_2O_4$ crystals further facilitate the Li^+ insertion capability and enhance the overall Li^+ storage capacity and cycle life.[41-43] The optimized unique hierarchically structured macroporous TiO_2 with inner-particle mesopores and the $Li_2Ti_2O_4$ nanocrystallites ensure the high reversible capacity, excellent rate capability and outstanding cycle performance.

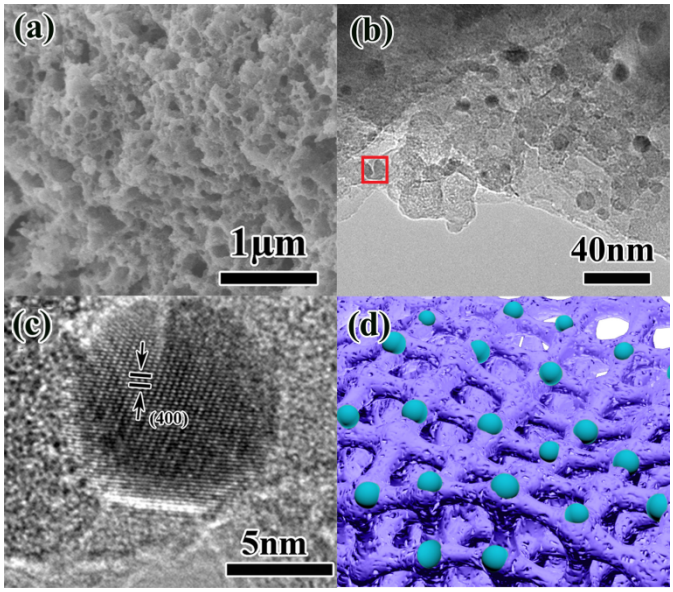

Figure 6. Low magnification (a) SEM and (b) TEM image,(c) HRTEM image from the area defined by the square in (b), and (d) schematic illustration of $Li_2Ti_2O_4$ nanoparticles in the RPC-P TiO_2 electrode after 1000 cycles at 2C.

4 Conclusions

In summary, we demonstrate a green and facile biomolecular self-assembly strategy to optimize 3D interconnected macroporous TiO_2 with inner-particle mesoporosity for advanced LIBs. The RPC-P TiO_2 exhibits a high initial coulombic efficiency, high capacity, long cycle life and superior electrochemical performance at high rates for several thousand cycles due to its stable, hierarchically macro-mesoporous structure and shortened path length to facilitate Li^+ diffusion and insertion. The remarkable electrochemical performance indicates that this unique 3D interconnected macro-mesoporous structure via biomolecular self-assembly is a promising anode material for high performance LIBs. Our work on biomolecular self-assembly of lipids and proteins from *rape pollen* coats would help to understand the complex natural self-assembly systems and to extend this green, facile and economical method into biotemplated synthesis for other materials for various applications, such as gas sensing, photocatalysis and photonics.

Acknowledgements

B. L. Su acknowledges the Chinese Central Government for an "Expert of the State" position in the Program of the "Thousand Talents". Y. Li acknowledges Hubei Provincial Department of Education for the "Chutian Scholar" program. T. Hasan acknowledges funding from RAEng fellowship (Graphlex) and EPSRC IAA grant EP/K503757/1(GRASS). G. Van Tendeloo and Z. Y. Hu acknowledge support from the EC Framework 7 program ESTEEM2 (Reference 312483). This work is realized in the frame of a program for Changjiang Scholars and Innovative Research Team (IRT_15R52) of Chinese Ministry of Education. This work is also financially supported by Hubei Provincial Natural Science Foundation (2014CFB160), International Science & Technology Cooperation Program of China (2015DFE52870) and Self-determined and Innovative Research Funds of the SKLWUT (2015-ZD-7). We also thank J. L. Xie, X. Q. Liu and T. T. Luo for TEM analysis from Research and Test Center of Materials at Wuhan University of Technology.

Notes and references

[1] Y. Xia, Z. Xiao, X. Dou, H. Huang, X. H. Lu, R. J. Yan, Y. P. Gan, W. J. Zhu, J. P. Tu, W. K. Zhang, *ACS Nano,* 2013, ***7***, 7083-7092.
[2] D. Deng, M. G. Kim, J. Y. Lee, J. Cho, *Energy Environ. Sci.,* 2009, ***2***, 818-837.
[3] W. Li, Z. X. Wu, J. X. Wang, A. A. Elzatahry, D. Y. Zhao, *Chem. Mater.,* 2013, ***26***, 287-298.
[4] Y. Ren, L. J. Hardwick, P. G. Bruce, *Angew. Chem. -Int. Edit.,* 2010, ***122***, 2624-2628.
[5] L. Kavan, J. Rathouský, M. Grätzel, V. Shklover, A. Zukal, *Micropor. Mesopor. Mater.,* 2001, ***44***, 653-659.
[6] P. Kubiak, T. Fröschl, N. Hüsing, U. Hörmann, U. Kaiser, R. Schiller, C. K. Weiss, K. Landfester, M. Wohlfahrt‐Mehrens, *Small,* 2011, ***7***, 1690-1696.
[7] H. E. Wang, H. Cheng, C. P. Liu, X. Chen, Q. L. Jiang, Z. G. Lu, Y. Y. Li, C. Chung, W. J. Zhang, J. A. Zapien, *J. Power Sources,* 2011, ***196***, 6394-6399.
[8] H. E. Wang, Z. G. Lu, L. J. Xi, R. G. Ma, C. D. Wang, J. A. Zapien, I. Bello, *ACS Appl. Mater. Interfaces,* 2012, ***4***, 1608-1613.
[9] P. Kubiak, J. Geserick, N. Hüsing, M. Wohlfahrt-Mehrens, *J. Power Sources,* 2008, ***175***, 510-516.
[10] F. Schüth, *Annu. Rev. Mater. Res.,* 2005, ***35***, 209-238.
[11] D. H. Chen, R. A. Caruso, *Adv. Funct. Mater.,* 2013, ***23***, 1356-1374.

[12] P. Zhu, Y. Z. Wu, M. V. Reddy, A. Sreekumarn Nair, B. V. R. Chowdari, S. Ramakrishna, *RSC Adv.*, 2012, ***2***, 531-537
[13] M. V. Reddy, X. W. Valerie Teoh, T. B. Nguyen, Y.Y Michelle Lim, B. V. R. Chowdari, *J. Electrochem. Soc.*, 2012, ***159***, A762-A769.
[14] M. V. Reddy, N. Sharma, S. Adams, R. Prasada Rao, V.K. Peterson, B. V. R. Chowdari, *RSC Adv.*, 2015, ***5***, 29535-29544.
[15] Y. Li, Z.Y. Fu, B.L. Su, *Adv. Funct. Mater.,* 2012, ***22***, 4634-4667.
[16] H. Zhou, T. X. Fan, D. Zhang, *ChemSusChem,* 2011, ***4***, 1344-1387.
[17] C. Sanchez, H. Arribart, M. M. G. Guille, *Nat. Mater.,* 2005, ***4***, 277-288.
[18] T. X. Fan, S. K. Chow, D. Zhang, *Prog. Mater. Sci.,* 2009, ***54***, 542-659.
[19] D. Murphy, *Protoplasma.,* 2006, ***228***, 31-39.
[20] F. Song, H. L. Su, J. J. Chen, W. J. Moon, W. M. Lau, D. Zhang, *J. Mater. Chem.,* 2012, ***22***, 1121-1126.
[21] F. Song, H. L. Su, J. Han, W. M. Lau, W. J. Moon, D. Zhang, *J. Phys. Chem. C,* 2012, ***116***, 10274-10281.
[22] S. G. Zhang, *Nat. Biotechnol.,* 2003, ***21***, 1171-1178.
[23] J. Jin, S. Z. Huang, J. Liu, Y. Li, D. S. Chen, H. E. Wang, Y. Yu, L. H. Chen, B. L. Su, *J. Mater. Chem., A* 2014, ***2***, 9699-9708.
[24] M. V. Reddy, S. Adams, G. T. J. Liang, I. F. Mingze, h.V. T. An, B. V. R. Chowdari, *Solid State Ionics*, 2014, ***262***, 120-123.
[25] P. cheng Wang, K. Yao, J. Zhu, X. Liu, T. ting Lu, M. Lu, *Catal. Commun.,* 2013, ***39***, 90-95.
[26] K. Sing, D. Everett, R. Haul, L. Moscou, R. Pierotti, J. Rouquerol, T. Siemieniewska, *Pure Appl. Chem.,* 1985, ***57***, 603-619.
[27] X. N. Li, Y. C. Zhu, X. Zhang, J. W. Liang, Y. T. Qian, *RSC Adv.,* 2013, ***3***, 10001-10006.
[28] G. L. Xu, Y. F. Xu, H. Sun, F. Fu, X. M. Zheng, L. Huang, J. T. Li, S. H. Yang, S. G. Sun, *Chem. Commun.,* 2012, ***48***, 8502-8504.
[29] X. W. Li, S. L. Xiong, J. F. Li, X. Liang, J. Z. Wang, J. Bai, Y. T. Qian, *Chem. Eur. J.,* 2013, ***19***, 11310-11319.
[30] Y. M. Sun, X. L. Hu, W. Luo, Y. H. Huang, *J. Mater. Chem.,* 2012, ***22***, 19190-19195.
[31] W. Luo, X. L. Hu, Y. M. Sun, Y. H. Huang, *ACS Appl. Mater. Interfaces,* 2013, ***5***, 1997-2003.
[32] M. V. Reddy, R. Jose, T. H. Teng, B. V. R. Chowdari, S. Ramakrishna, *Electrochimi. Acta*, 2010, ***55***, 3109-3117
[33] L. J. Fu, T. Zhang, Q. Cao, H. P. Zhang, Y. P. Wu, *Electrochem. Commun.,* 2007, ***9***, 2140-2144.
[34] H. L. Jiang, X. L. Yang, C. Chen, Y. H. Zhu, C. Z. Li, *New J. Chem.,* 2013, ***37***, 1578-1583.
[35] M. V. Reddy, B. L. W. Wen, K. P. Loh, B. V. R. Chowdari, *ACS Appl. Mater. Interfaces*, 2013, ***5***, 7777-7785.
[36] M. V. Reddy, G. Pirthvi, K. P. Loh, B. V. R. Chowdari, *ACS Appl. Mater. Interfaces*, 2014, ***6***, 680-690.
[37] M. V. Reddy, S. Madhavi, G. V. Subba Rao, B. V. R. Chowdari, *J. Power Sources*, 2006, ***162***, 1312-1321
[38] X. L. Wu, Y. G. Guo, J. Su, J. W. Xiong, Y. L. Zhang, L. J. Wan, *Adv. Energy Mater.,* 2013, ***3***, 1155-1160.
[39] Q. Gao, M. Gu, A. Nie, F. Mashayek, C. M. Wang, G. M. Odegard, R. Shahbazian Yassar, *Chem. Mater.,* 2014, ***26***, 1660-1669.
[40] R. Cava, D. Murphy, S. Zahurak, A. Santoro, R. Roth, *J. Solid State Chem.,* 1984, ***53***, 64-75.
[41] J. Jin, S. Z. Huang, J. Liu, Y. Li, L. H. Chen, Y. Yu, H. E. Wang, C. P. Grey, B. L. Su, *Adv. Sci.,* 2015, ***2***, 1500070.
[42] J. Jin, S. Z. Huang, Y. Li, H. Tian, H. E. Wang, L. H. Chen, Y. Yu, T. Hasan, B. L. Su, *Nanoscale,* 2015, ***7***, 12979-12989.
[43] J. Jin, S. Z. Huang, J. Shu, H. E. Wang, Y. Li, Y. Yu, L. H. Chen, B. J. Wang, B. L. Su, *Nano Energy,* 2015, ***16***, 339-349.

Supporting Information

3D Interconnected Hierarchically Macro-mesoporous TiO_2 Network Optimized by Biomolecular Self-assembly for High Performance Lithium Ion Battery

Xiao-Ning Ren,[†a] Liang Wu,[†a] Jun Jin,[a] Jing Liu,[a] Zhi-Yi Hu,[b] Yu Li,[*a] Tawfique Hasan,[c] Xiao-Yu Yang,[a] Gustaaf Van Tendeloo[b] and Bao-Lian Su[*a,d,e]

[a]*Laboratory of Living Materials at the State Key Laboratory of Advanced Technology for Materials Synthesis and Processing, Wuhan University of Technology, 122 Luoshi Road, 430070, Wuhan, Hubei, China; Email: yu.li@whut.edu.cn; baoliansu@whut.edu.cn.*

[b] *EMAT (Electron Microscopy for Materials Science), University of Antwerp, 171 Groenenborgerlaan, B-2020 Antwerp, Belgium.*

[c] *Cambridge Graphene Centre, University of Cambridge, 9 JJ Thomson Avenue, Cambridge CB3 0FA, United Kingdom*

[d]*Laboratory of Inorganic Materials Chemistry (CMI), University of Namur, 61 rue de Bruxelles, B-5000 Namur, Belgium; E-mail: bao-lian.su@unamur.be*

[e]*Department of Chemistry and Clare Hall, University of Cambridge, Cambridge CB21 EW, United Kingdom; E-mail: bls26@cam.ac.uk*

† These two authors contributed equally to this work.

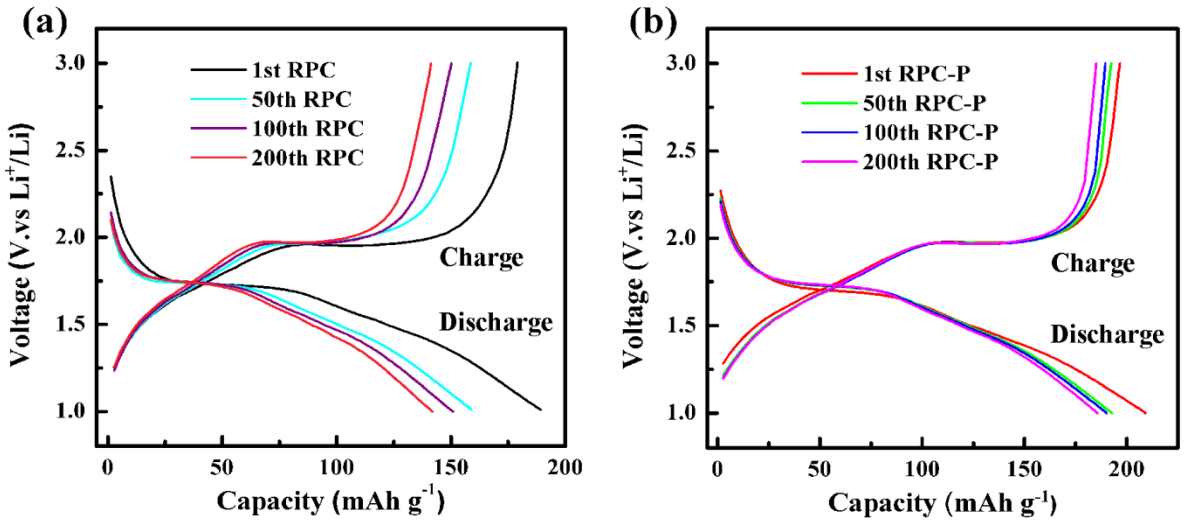

Figure S1. Charge and discharge curves of (a) RPC TiO_2 and (b) RPC-P TiO_2 at the 1st, 50th, 100th and 200th cycle at 1C.

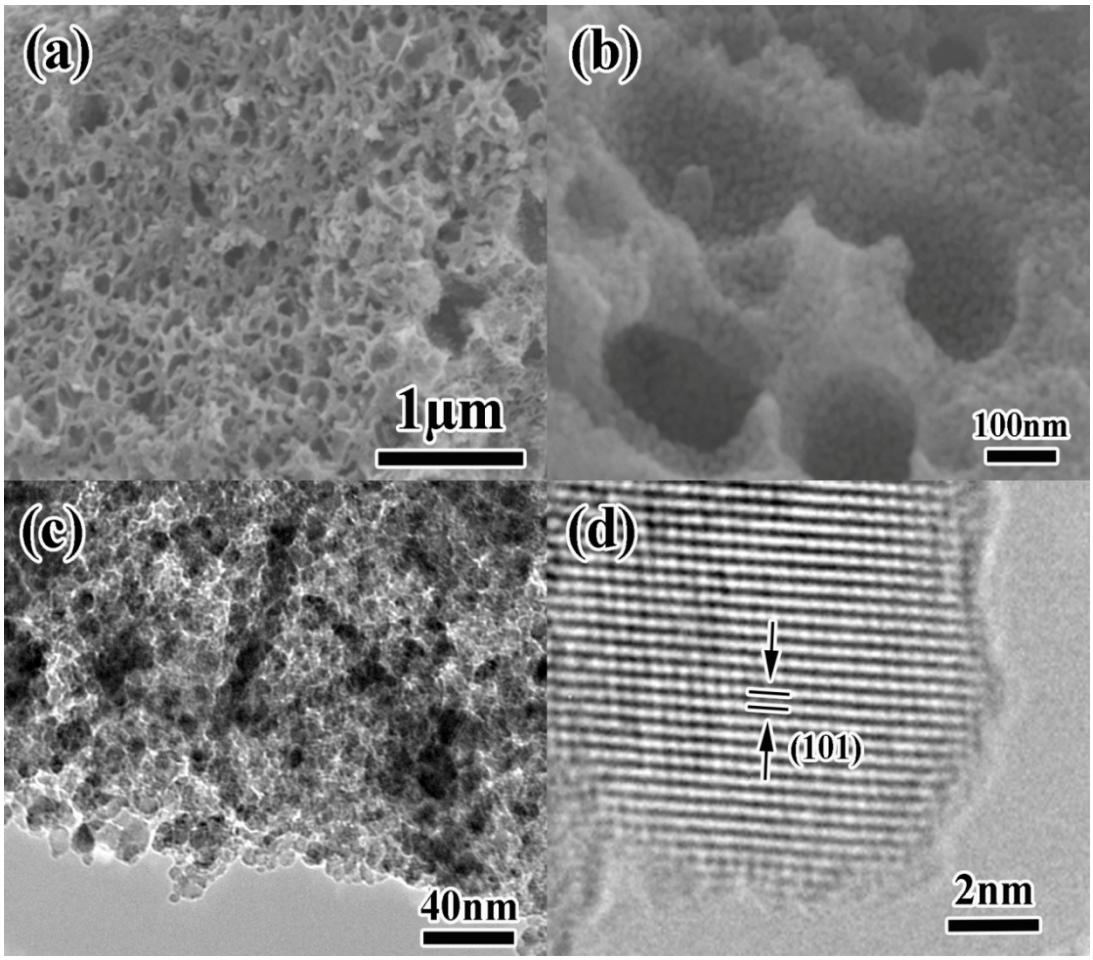

Figure S2. (a,b) SEM images and (c,d) TEM images of the as-prepared RPC TiO_2. The SEM image in (a) clearly shows the macroporous structure. The SEM image in (b) displays the nanoparticles constructed the walls. The TEM image in (c) reveals the inter-particles mesopores (also called worm-like mesopores). The HRTEM image presents the (101) crystal plane of one anatase nanoparticle.

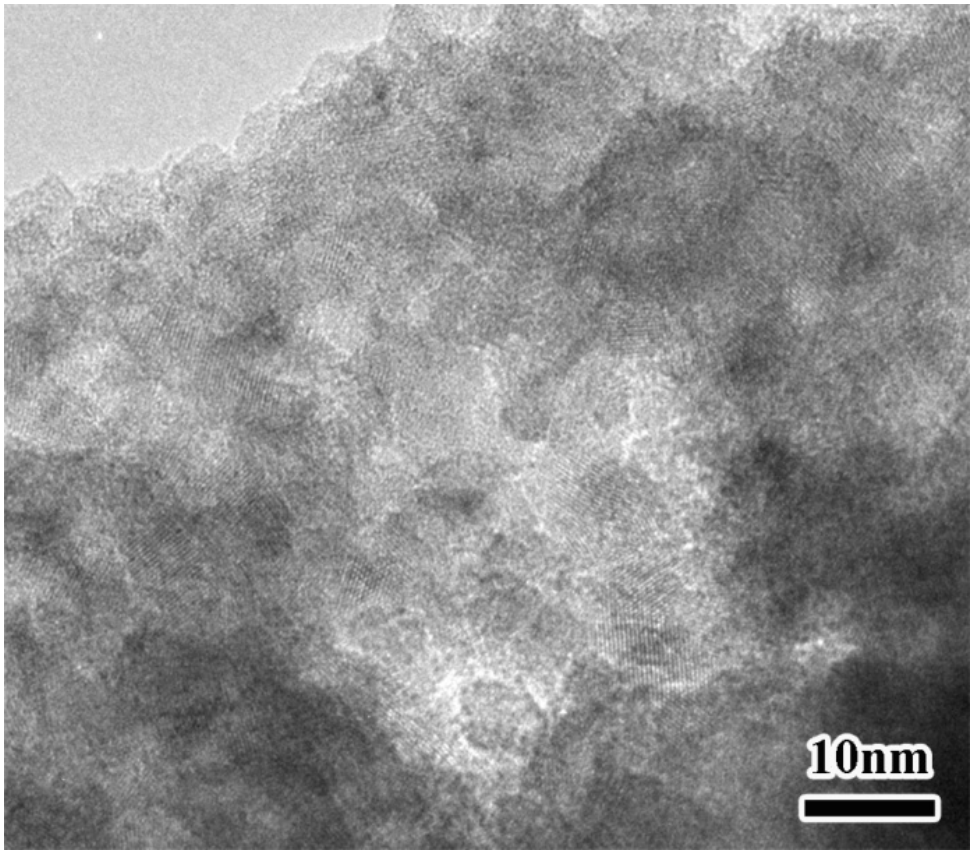

Figure S3. The HRTEM image of RPC-P TiO_2 at 2C after 1000 cycles, clearly demonstrating the remained inner-particle mesopores.